Loss of αB-crystallin function in zebrafish reveals critical roles in the development of the lens and stress resistance of the heart

Received for publication, July 25, 2017, and in revised form, November 17, 2017 Published, Papers in Press, November 21, 2017, DOI 10.1074/jbc.M117.808634

Sanjay Mishra[‡1], Shu-Yu Wu[‡1], Alexandra W. Fuller[‡], Zhen Wang[§¶], Kristie L. Rose[§¶], Kevin L. Schey[§¶], and Hassane S. Mchaourab[‡2]

From the Departments of [‡]Molecular Physiology and Biophysics and [§]Biochemistry and [¶]Mass Spectrometry Research Center, Vanderbilt University School of Medicine, Nashville, Tennessee 37232

Edited by Xiao-Fan Wang

Genetic mutations in the human small heat shock protein αB-crystallin have been implicated in autosomal cataracts and skeletal myopathies, including heart muscle diseases (cardiomyopathy). Although these mutations lead to modulation of their chaperone activity *in vitro*, the *in vivo* functions of αB-crystallin in the maintenance of both lens transparency and muscle integrity remain unclear. This lack of information has hindered a mechanistic understanding of these diseases. To better define the functional roles of αB-crystallin, we generated loss-of-function zebrafish mutant lines by utilizing the CRISPR/Cas9 system to specifically disrupt the two αB-crystallin genes, *αBa* and *αBb*. We observed lens abnormalities in the mutant lines of both genes, and the penetrance of the lens phenotype was higher in *αBa* than *αBb* mutants. This finding is in contrast with the lack of a phenotype previously reported in αB-crystallin knock-out mice and suggests that the elevated chaperone activity of the two zebrafish orthologs is critical for lens development. Besides its key role in the lens, we uncovered another critical role for αB-crystallin in providing stress tolerance to the heart. The αB-crystallin mutants exhibited hypersusceptibility to develop pericardial edema when challenged by crowding stress or exposed to elevated cortisol stress, both of which activate glucocorticoid receptor signaling. Our work illuminates the involvement of αB-crystallin in stress tolerance of the heart presumably through the proteostasis network and reinforces the critical role of the chaperone activity of αB-crystallin in the maintenance of lens transparency.

αB-crystallin (Cryab or HspB5) is a small heat shock protein (sHSP)[3] that is expressed in multiple tissues and organs, including the lens, heart, and skeletal muscles (1, 2), and can be transcriptionally induced by stress through the binding of heat shock transcription factor 1 (Hsf1) to a heat-shock element in its promoter (3). Although initially characterized by its function as a molecular chaperone (4–7), αB-crystallin appears to have physiological roles that transcend the non-specific binding of destabilized proteins (8, 9). For example, it has been associated with the integrity of Desmin, implicated in binding of Titin in the heart and intermediate filaments in the lens (10–12), and more recently in direct regulation of Argonaute2 (13).

The diversity of its molecular targets endows αB-crystallin with a pivotal role in the physiology of the heart and transparency of the lens (1). Indeed, a number of mutations in αB-crystallin have been associated with severe pathologies of the lens, heart, and skeletal muscles (14–16), including the R120G mutation, which is associated with Desmin-related myopathy in humans (17). Although the detailed mechanisms by which these mutations lead to pathology are not fully delineated, they collectively suggest a critical role for this protein in signaling networks that safeguard and maintain cellular proteostasis (1).

αB-crystallin shares many of the properties of vertebrate sHSPs, including the presence of the highly conserved α-crystallin domain in its sequence, a flexible C-terminal extension and a hydrophobic N-terminal segment (18–21). Whereas structures of isolated α-crystallin domain dimers have been determined, the native oligomer assembly has proved refractory to high resolution structures because of its polydispersity and dynamics, properties that are shared by many mammalian sHSPs (22, 23). The αB-crystallin oligomers undergo subunit exchange mediated by dissociation into smaller multimers, likely dimers (24). In general, the polydispersity and dynamics of the sHSP oligomers are critical for regulation of *in vitro* chaperone function (21, 25–30). Phosphorylation of αB-crystallin in response to stress and during aging activates its chaperone function presumably through changes in its oligomer size and/or the rate of subunit exchange (7, 31–33).

This work was supported by National Institutes of Health Grants R01 EY12018 (to H. M.), P30 EY008126 (to H. M. and K. L. S.), and the Clinical and Translational Science Award UL1 RR024975-01, from the Vanderbilt University Proteomics Facility in the Mass Spectrometry Research Center, and the Vanderbilt University School of Medicine Cell Imaging Shared Resource. The authors declare that they have no conflicts of interest with the contents of this article. The content is solely the responsibility of the authors and does not necessarily represent the official views of the National Institutes of Health.

This article contains Tables S1–S4 and Movies S1 and S2.

[1] Both authors contributed equally to this work.

[2] To whom correspondence should be addressed. E-mail: hassane.mchaourab@vanderbilt.edu.

[3] The abbreviations used are: sHSP, small heat shock protein; GR, glucocorticoid receptor; dpf, days post-fertilization; WMISH, whole-mount *in situ* hybridization; WSF, water-soluble fraction; WIF, water-insoluble fraction; PSC, posterior subcapsular cataract; MMTS, methyl methanethiosulfonate; NMD, nonsense-mediated mRNA decay; MO, morpholino; qRT, quantitative RT; iTRAQ, isobaric tags for relative and absolute quantitation; PTU, 1-phenyl-2-thiourea.

Table 1
Mutation alleles of αB-crystallin genes generated by CRISPR/Cas9

Allele	Predicted polypeptide sequence (native residues are underlined)	Predicted polypeptide length
Cryaba^{5bpINS}	MEISIQHPWS WIADPCSQAS SLIEFLISIL ESIYLTVTLF HLSTPCFTIV LICGAFQAGG TVACRR	66
Cryaba^{15bpDEL}	Δ^{10}YRRPL^{14}	163
Cryaba^{35bpDEL}	MEISIQHPLS NF	12
Cryabb^{2bpINS}	MDIAITIPRS GASYFLSSFP AGNLGSILLR PM	32
Cryabb^{10bpDEL}	MDIARSGASY FLSSFPAGNL GSILLRPT	28
Cryabb^{8bpDEL}	MDIAINPPFR RILFPIFFPR RQFGEHITEA DVISSPTIFL SSQSKLDGKR SF	52
Cryabb^{3bpDEL}	MDIAINPPFR RILFPIFFPR RQFGEHITEA DVISSLSQRS SFLRSPSWME SGVSEVSYKK LVFSGF	66

Although a role of αB-crystallin in the proteostasis network is well established and its involvement in the physiology and homeostasis of multiple tissues is supported by direct evidence, a detailed understanding of the molecular mechanisms underlying these roles has yet to emerge. An attempt to generate a knock-out mouse line was confounded by the inadvertent knock-out of HspB2, another sHSP with a presumed role in the development of muscle tissues (34). Although the knock-out mice developed progressive myopathy into adulthood (34), disentangling the contributions of the two sHSPs has proven challenging (35, 36).

Here, we capitalize on the intrinsic advantages of the zebrafish as a vertebrate model system to carry out a detailed investigation of the consequences of αB-crystallin loss of function on lens and heart developments. We find that although disruption of the two αB-crystallin genes leads to lens defects, they are not essential for cardiac development under normal rearing conditions. Rather, a novel role of αB-crystallins is uncovered under stress conditions, specifically in response to glucocorticoid receptor (GR) signaling. Zebrafish lines, deficient of either αB-crystallin, show the development of cardiac edema when embryos are subjected to crowding conditions or challenged with GR agonists. Together, our results provide novel insights on the physiological roles of vertebrate αB-crystallins.

Results

Generation of αB-crystallin loss-of-function alleles by CRISPR/Cas9 system

With the goal of defining the physiological roles of αB-crystallin and linking them to its well-understood chaperone mechanism, we have taken advantage of the CRISPR/Cas9 technology (37–39) to generate zebrafish mutant lines where the two αB-crystallin orthologs, *cryaba* and *cryabb*, have been disrupted (hereafter, we use the nomenclature "αBa" and "αBb" for simplicity). We successfully generated multiple alleles carrying various deletions or insertions for each gene (summarized in Table 1; see details under "Experimental procedures") and a few alleles were subsequently propagated after confirmation of the mutations by DNA sequencing (Fig. 1*A*). For the rest of this study, we focus only on the $\alpha Ba^{35bpDEL}$ and $\alpha Bb^{10bpDEL}$ mutant alleles (Fig. 1*B*), given that both are predicted to encode extremely truncated polypeptides and are expected to function as null alleles. Henceforth, these deletion mutations, $\alpha Ba^{35bpDEL}$ and $\alpha Bb^{10bpDEL}$, are referred to as $\alpha Ba^{-/-}$ and $\alpha Bb^{-/-}$.

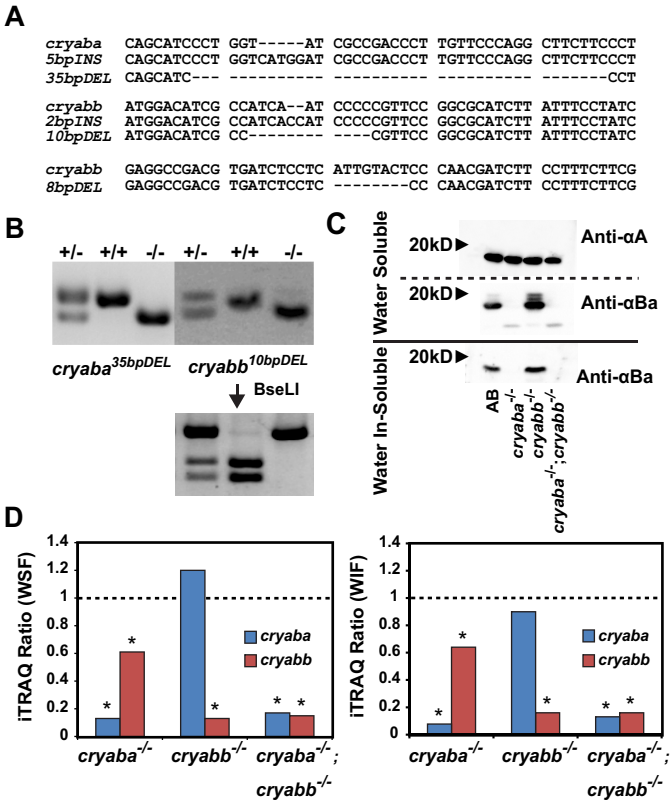

Figure 1. Generation of knock-out alleles of αB-crystallin genes by CRISPR/Cas9. *A,* alignment of the DNA sequences of the mutant alleles of *αBa* and *αBb*. *B,* electrophoresis of the genomic DNA of the adult zebrafish amplified by PCR: $\alpha Ba^{35bpDEL}$ on 3% agarose gel and $\alpha Bb^{10bpDEL}$ on 4% agarose gel. The genotyping of $\alpha Bb^{10bpDEL}$ allele was confirmed by digestion with restriction enzyme BseLI. *C,* Western immunoblot of the water-soluble and water in-soluble protein fraction of the excised lenses of the adult zebrafish. After transfer on nitrocellulose membrane, proteins were probed with polyclonal antibody against zebrafish Cryaa (αA) or zebrafish Cryaba (αBa). *D,* αB-crystallin iTRAQ ratios in the lens of both $\alpha Ba^{-/-}$ and $\alpha Bb^{-/-}$ adult fishes. The *left panel* shows iTRAQ ratios of αBa and αBb in mutant animals compared with wild-type animals in the lens WSF, and the *right panel* shows the same from the WIF.

To confirm the loss of the αB proteins in αB-crystallin mutant lines, we utilized iTRAQ-based proteomics (40) to quantify the relative changes in the abundance of αB proteins in the adult lens of $\alpha Ba^{-/-}$ and $\alpha Bb^{-/-}$. In both water-soluble (WSF) and -insoluble (WIF) fractions, we observed that compared with WT, the relative abundance of native αB peptides in each respective mutant was reduced significantly to a marginally-detectable level (Fig. 1*D*). Additionally, we generated polyclonal antibodies against purified zebrafish αA- and αBa-crys-

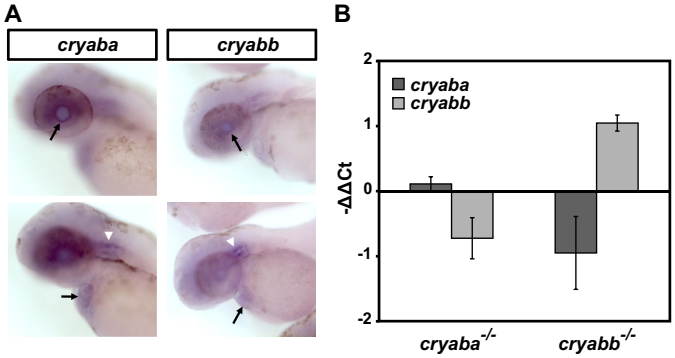

Figure 2. Expression profiles of αB-crystallin genes. *A,* expression pattern of *αBa* and *αBb* genes by whole-mount *in situ* hybridization. *Black arrows* indicate lens (*top row*) and heart (*bottom row*). *White arrowheads* indicate otic vesicles. *B,* relative expression changes of *αBa* and *αBb* genes in *αBa* and *αBb* homozygous mutants, as measured by qRT-PCR.

tallin proteins, and we probed crude protein extracts from the lens of mutant fish lines. Although the level of αA-crystallin was not affected by the loss of either αBa or αBb (Fig. 1*C*, *Anti-αA*), we confirmed the loss of αBa-crystallin in the lens of both $αBa^{-/-}$ and the double mutant, $αBa^{-/-}$;$αBb^{-/-}$ (both WSF and WIF; Fig. 1*C*). Interestingly, using the αA Western blotting signal to normalize expression levels in the $αBb^{-/-}$ lens, we observed a slight increase of αBa protein in the WSF of the $αBb^{-/-}$ lens, which was in agreement with our iTRAQ data (Fig. 1*D*), suggesting a possible compensatory response to the loss of αBb protein. Moreover, we observed mobility shifts of the αBa band in the WSF (but not in WIF) of the lens (anti-αBa; in WT and $αBb^{-/-}$) that likely represent post-translational modifications, such as phosphorylation or acetylation (32, 41, 42). These supershifted bands were particularly noticeable in the $αBb^{-/-}$ lens, which might suggest an increase in the amount of post-translational modification of αBa-crystallin. We are currently pursuing the molecular nature of these shifted species and trying to determine whether they are phosphatase-sensitive.

αB-crystallins are expressed in both the lens and heart during zebrafish embryogenesis

Previously, we showed that both αBa and αBb are expressed in zebrafish embryos from as early as 2 dpf (43). To determine their spatial expression pattern, we performed whole-mount RNA *in situ* hybridization (WMISH) for αBa and αBb on 2-dpf embryos according to the established protocol (44). As expected, we observed the expression of αBa and αBb in the lens of 2-dpf embryos, as well as in the hearts, albeit with lower staining signal (Fig. 2*A*, *black arrows*). In addition, both genes were broadly expressed in the brain region and showed particularly enriched expression in the otic vesicles (Fig. 2*A*, *white arrowheads*).

We explored whether a compensatory transcriptional regulation exists between the two paralogs of αB genes in the reciprocal mutants, which is often found in duplicated genes (45). However, we observed no significant change (<1.6 cycle difference (46)) of αBb expression in αBa mutant embryos and vice versa (Fig. 2*B*). In contrast, we did not observe nonsense-mediated mRNA decay (NMD) for αBa or αBb mRNA transcripts

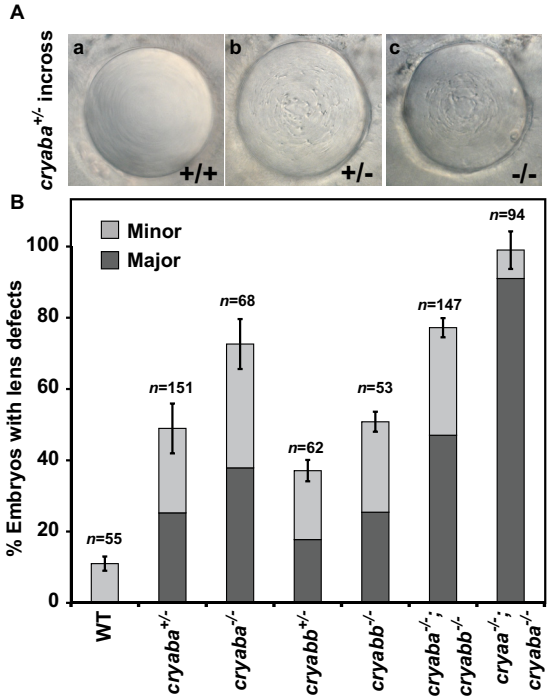

Figure 3. Lens defects in zebrafish αB-crystallin mutant embryos. *A,* representative images of lens phenotypes in WT and *αBa* homo-/heterozygotes. *B,* comparison of percentage of embryos showing lens defects between WT and αB-crystallin homo-/heterozygous mutants (*αBa* and *αBb*), as well as αB-crystallin double mutants and αA-/αB-crystallin double mutants.

that were derived from their respective mutant alleles, even though they are expected to behave as protein null (Fig. 2*B*). Nonetheless, as shown in our Western blot analysis, the retained αBa mRNA did not produce a detectable amount of αBa protein (Fig. 1*C*), which further supported that the αBa mutation is a loss-of-function allele.

Loss-of-function of αB-crystallin causes lens defects in zebrafish

Consistent with our previous demonstration that knockdown of *αBa* and *αBb* by morpholinos can perturb lens transparency in zebrafish (43), the loss of αB-crystallin function, either *αBa* or *αBb*, led to apparent abnormalities in the embryonic lens starting at 3 dpf which became evident at 4 dpf (Fig. 3*A*), while the overall morphology of the embryos remained normal. The nature of these lens defects was similar to those previously described for αB-crystallin morphants or αA-crystallin knock-out lines ($αA^{-/-}$) (43). Following the same classification system previously established, lens defects were categorized into three classes based on the severity: "Major" (Fig. 3*A*, *panels b* and *c*), "Minor" (data not shown), and "WT-like" class" (Fig. 3*A*, *panel a*) (43). Initially, we noted that the incidence of lens defects in the offspring derived from heterozygote incrosses, both minor and major classes, occurred in a frequency inconsistent with the lens phenotype being strictly recessive (>25%). Genotyping of phenotypic embryos revealed that both the minor and major phenotypes occur in heterozygous and homozygous mutants (data not shown). Similar to $αA^{-/-}$ embryos, both *αBa* and *αBb* homozygous mutants ($αBa^{-/-}$ and $αBb^{-/-}$) showed lens defects with a range of

severity. Greater penetrance and severity of lens defects were observed in $\alpha Ba^{-/-}$ embryos. For $\alpha Ba^{-/-}$, ~75% of the total embryos presented lens defects, and 38% were of the major class, whereas ~50% of the $\alpha Bb^{-/-}$ embryos showed lens abnormalities and 25% were of the major class (Fig. 3*B*). These results suggested that *αBa* might play a more important role than *αBb* in the maintenance of zebrafish lens transparency. Interestingly, a gene dosage effect was observed in *αBa* and *αBb* genes. When we crossed homozygous *αBa* mutant adult with WT fish ($\alpha Ba^{-/-} \times$ WT), the resulting heterozygous αBa mutant embryos ($\alpha Ba^{+/-}$) exhibited reduced lens defects (~48%), relative to $\alpha Ba^{-/-}$ embryos. A similar effect was observed for $\alpha Bb^{-/-}$ embryos, in which ~37% of them showed lens defects (Fig. 3*B*).

Because both *αBa* and *αBb* mutants were adult-viable, we generated *αBa*/*αBb* double mutants ($\alpha Ba^{-/-};\alpha Bb^{-/-}$) to determine whether a higher penetrance of the lens phenotypes would be observed by complete elimination of αB-crystallin. Compared with the single mutant, particularly $\alpha Ba^{-/-}$, the frequency of major lens defects increased moderately in *αBa*/*αBb* double mutants (by about 10%), but the overall penetrance was not significantly changed, consistent with the conclusion that *αBa* plays a more prominent role in lens development than *αBb* (Fig. 3*B*).

Although both *αA* and *αBa* appear critical for proper lens formation, the penetrance and severity of the phenotypes vary in the single knock-out lines. Therefore, we generated a double loss-of-function line by crossing $\alpha Ba^{-/-}$ fish with the $\alpha A^{-/-}$ line generated in our earlier work (43), and we examined the occurrence of the lens defects. To avoid the protective effect of maternal *αA* expression, $\alpha A^{-/-};\alpha Ba^{-/-}$ embryos were derived from $\alpha A^{-/-};\alpha Bb^{-/-}$ adult incross, and as expected, they exhibited an almost complete penetrance (~99%), with ~90% of lens defects belonging to the major class (Fig. 3*B*).

αB-crystallin mutants showed stress-induced cardiac phenotypes

In addition to its role in the lens, αB-crystallin has been implicated in the cellular integrity of the cardiomyocytes through interactions with Titin and Desmin (11, 17, 47). Therefore, we examined whether *αBa* mutants exhibited abnormalities in heart development by incrossing either $\alpha Ba^{+/-}$ or $\alpha Ba^{-/-}$. The resulting embryos from both crosses displayed morphologically normal hearts (Fig. 4*A*, *panels a* and *b*) under routine collection and regular embryo-rearing conditions (28.5 °C, in 35-mm Petri dish, up to 5–6 dpf). Similar results were observed in *αBb* mutants (both $\alpha Bb^{+/-}$ and $\alpha Bb^{-/-}$). These results contradict a previous study reporting that knocking down *αBa* and *αBb* genes by morpholinos would lead to heart failure and skeletal muscle defects in zebrafish embryos (48). Given the prevalent non-specific effects and the reported unreliability of using morpholino to interfere with gene functions (49), we conclude that αB-crystallin genes are largely dispensable for muscle and heart development during embryogenesis. Indeed, αB-crystallin double mutant fishes ($\alpha Ba^{-/-};\alpha Bb^{-/-}$) are viable and fertile as adults. Raising the progenies derived from an $\alpha Ba^{+/-}$ or $\alpha Bb^{+/-}$ adult incross, we found that the ratio of either $\alpha Ba^{-/-}$ or $\alpha Bb^{-/-}$ progeny that survived to adulthood (>3 months old) was in accordance with Mendelian ratio (Table 3). Moreover, the $\alpha Ba^{-/-}$ and $\alpha Bb^{-/-}$ adults did not exhibit lower survival rate compared with siblings under normal housing conditions for at least 10 months (Table 3). These data further suggested that neither αB-crystallin gene is essential for zebrafish overall viability.

Although αB-crystallin-deficient embryos showed no apparent cardiac phenotype under the normal rearing conditions described above, we examined whether αB-crystallin is involved in the stress tolerance of the zebrafish developing heart. As a member of sHSPs, αB-crystallin has been shown to be inducible by various cellular stresses, including oxidative, genotoxic, and heat shock stresses (33, 50–52). Therefore, we raised 1 dpf αB-crystallin mutant ($\alpha Ba^{-/-}$ and $\alpha Bb^{-/-}$) embryos in high density (75 embryos per well of a 6-well plate; see "Experimental procedures" for detail) to simulate a "stressed" condition or a non-permissive condition induced by crowding, whereas controls from the same clutch were stocked at normal/non-stressed density (15 embryos per well of a 6-well plate). The gross morphology and heart development of the embryos were monitored daily until 5 dpf. Compared with the control embryos, the αB-crystallin mutant embryos subjected to crowding stress progressively developed pericardial edema with moderate penetrance (Fig. 4, *A* and *B*; $\alpha Bb^{-/-}$ shown here but similar phenotypes were observed in $\alpha Ba^{-/-}$), which becomes more evident at 4 dpf (Fig. 4*A*, *panels c* and *d*). In contrast, no such cardiac phenotype was detectable in the control (non-stressed) αB-crystallin mutant embryos (Fig. 4*A*, *panels a* and *b*). These cardiac phenotypes were very similar to what has been described previously in embryonic lethal mutants that developed cardiomyopathy, such as *titin* mutants (53). The stress-induced pericardial edema in αB-crystallin mutants was not reversible, as we were unable to raise those $\alpha Ba^{-/-}$ and $\alpha Bb^{-/-}$ embryos showing cardiac phenotypes to adulthood (none survived before reaching the juvenile stage; data not shown).

Interestingly, in addition to cardiac phenotypes, the lens defects shown in both $\alpha Ba^{-/-}$ and $\alpha Bb^{-/-}$ embryos were also influenced by crowding stress (Fig. 4*C*). Compared with the non-stressed condition (control), we observed higher penetrance of overall lens defects in $\alpha Ba^{-/-}$ (~20% increase) and $\alpha Bb^{-/-}$ (~12% increase) under the crowded rearing conditions.

Sensitivity of αB-crystallin mutants to crowding stress is mediated by glucocorticoid levels

Based on the observation that crowding causes phenotypic enhancement in two distinct tissues, we hypothesized that the underlying stress may be mediated by a systemic and intrinsic factor. Crowding stress of adult zebrafish has been shown to increase the body cortisol level (54, 55). Indeed, we examined the changes of the expression of known GR signaling downstream genes (*fkbp5*, *pxr*, and *pepck*) (56) in embryos raised under crowding conditions for 2 days, and we found that although all three genes showed trends of increased expression, only *pepck* was significantly up-regulated (Fig. 4*D*), which was consistent with the finding that *pepck* is a more sensitive GR signaling reporter gene during embryonic stages (56).

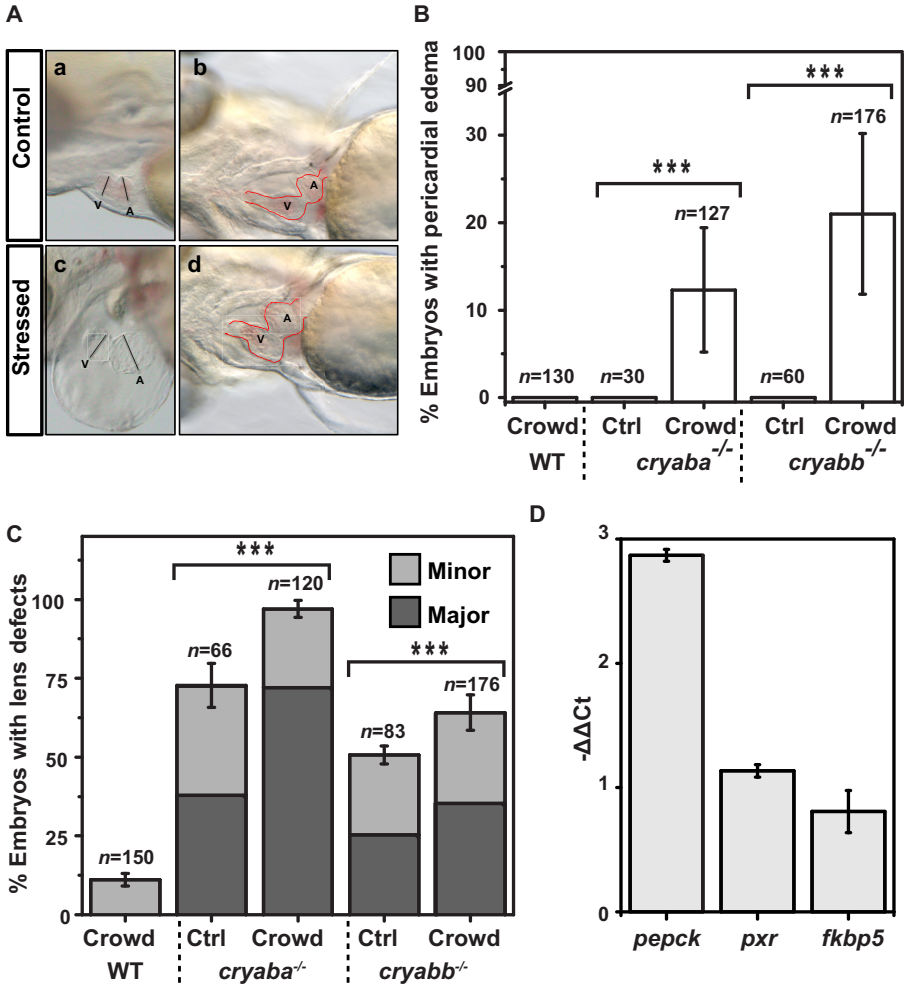

Figure 4. Stress-induced cardiac phenotypes in αB-crystallin mutant embryos. *A,* representative images of cardiac phenotypes in αB-crystallin mutant embryos: *panels a* and *b,* control/non-stressed; *panels c* and *d,* subjected to crowding stress. *A,* atrium; *V,* ventricle. *Red dotted line* demarcates the heart morphology. *B,* percentage of αB-crystallin mutant embryos showing pericardial edema under crowding stress. *C,* percentage of embryos showing lens defects in αB-crystallin mutants ($\alpha Ba^{-/-}$ and $\alpha Bb^{-/-}$) was influenced by the crowding stress. *D,* relative expression changes of GR signaling target genes (*pepck*, *pxr*, and *fkbp5*) in 3-dpf WT embryos after being raised in crowding conditions for 2 days (from 1 to 3 dpf), as measured by qRT-PCR.

Earlier reports have shown that the cardiac performance of zebrafish embryos declined when exposed to elevated cortisol levels (57). Therefore, we tested whether the αB-crystallin mutants lower the tolerance of the heart to cortisol, which is the main glucocorticoid stress hormone. For this purpose, the αB-crystallin mutant embryos were challenged with two different synthetic glucocorticoids, dexamethasone and hydrocortisone, to mimic the elevation of stress hormone level and overactivation of GR signaling. The αB-crystallin mutants ($\alpha Ba^{-/-}$; $\alpha Bb^{-/-}$ and $\alpha Ba^{-/-}$;$\alpha Bb^{-/-}$), treated with both GR agonists from 1 to 4 dpf, developed pericardial edema and dilated cardiac chambers (Fig. 5, *A* and *C*, *panels e* and *f*), similar to the phenotypes under the crowding stress (Fig. 4*A*). In contrast, non-treated αB-crystallin mutants (DMSO control) or WT embryos subjected to the same regimen of synthetic glucocorticoids mostly remained normal (Fig. 5*B*). As expected, the αA-crystallin mutants (43) did not exhibit cardiac abnormality when subjected to the crowding stress and dexamethasone treatment (Fig. 6*D*), which emphasize the distinct involvement of αB-crystallin in the maintenance of cardiac function. Together, these results clearly suggested that without the presence of αB-crystallin (*i.e.* loss-of-function), the embryonic heart is more vulnerable to increase in GR signaling activity.

Early cardiac development is unperturbed but cardiac functions appear compromised in αB-crystallin mutants when challenged with stress

We examined whether the heart phenotypes were a result of failures of cell fate specification by immunostaining of the ventricle and atrium. Compared with WT, both non-stressed $\alpha Bb^{-/-}$ embryos (and $\alpha Ba^{-/-}$) at 2 dpf showed largely normal specification and partition of the cardiac chambers (Fig. 5*C*, *panels a* and *b*; data not shown), consistent with the notion that αB-crystallin genes are not required for early cardiac development. Because cell death/apoptosis has been implicated in the αB-crystallin-associated cardiomyopathy, we performed TUNEL assay on both $\alpha Bb^{-/-}$ and $\alpha Ba^{-/-}$ embryos at 2 dpf and found no evidence of increased cell death in the heart, which suggested that apoptosis is not involved in the stress-induced heart phenotypes described above (Fig. 5*C*, *panels c* and *d*).

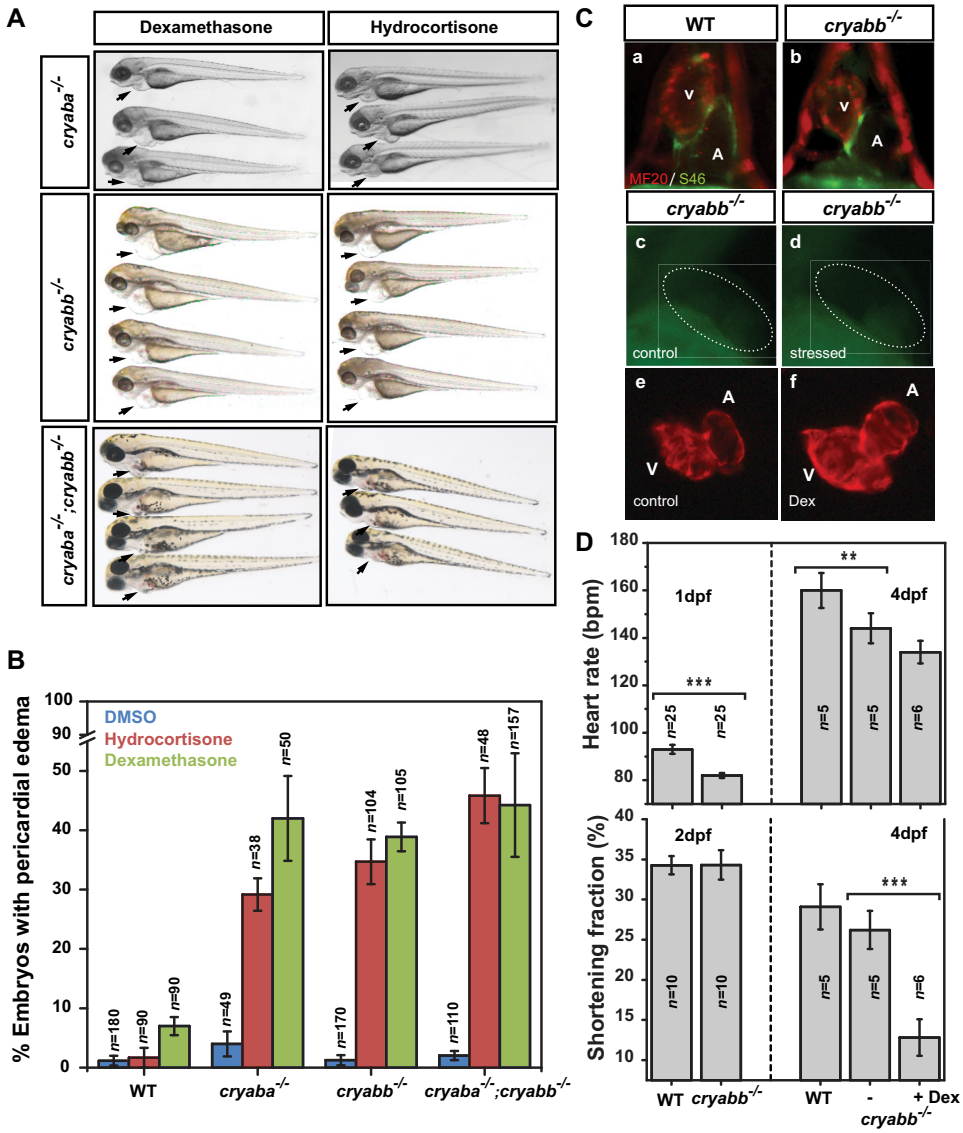

Figure 5. Overactivation of glucocorticoid signaling induced cardiac phenotypes in αB-crystallin mutant embryos. *A*, $\alpha Bb^{-/-}$ embryos showed pericardial edema when treated with GR agonists, dexamethasone (50 μM) and hydrocortisone (50 μM). *B*, percentage of $\alpha Bb^{-/-}$ embryos showing pericardial edema when treated with dexamethasone and hydrocortisone. *C*, immunofluorescence with MF20 and S46 antibodies allowed visualization of the ventricle (*red*) and atrium (*green*) in WT and $\alpha Bb^{-/-}$ embryos at 2 dpf (*panels a* and *b*). The TUNEL staining revealed no significant increase of apoptosis in the heart (*dotted circle area*) of 2-dpf $\alpha Bb^{-/-}$ embryos subjected to crowding compared with control $\alpha Bb^{-/-}$ embryos (*panels c* and *d*). The cardiac chambers of 4 dpf $\alpha Bb^{-/-}$ embryos were dilated after treating with dexamethasone (*Dex*) (*panels e* and *f*). *D*, *upper panel*, heart rates of WT, $\alpha Bb^{-/-}$ embryos (1 and 4 dpf), and $\alpha Bb^{-/-}$ embryos treated with dexamethasone (4 dpf). *Lower panel*, ventricular shortening fraction of WT, $\alpha Bb^{-/-}$ embryos (2 and 4 dpf), and $\alpha Bb^{-/-}$ embryos treated with dexamethasone (4 dpf).

Even though the early heart development appeared to be unaffected in αB-crystallin mutants, taking advantage of the embryos' optical transparency, we performed time-lapse imaging to monitor the heart rate and contraction dynamics of *αBb* mutants, without stress. We found that, compared with the WT, *αBb* mutants exhibited a slower heart rate (~10% decrease) at 1 dpf and the heart rate of *αBb* mutants remained lower at 4 dpf (Fig. 5*D*, *upper panel*). The ventricular shortening fraction, which can be used as an estimate of myocardial contractility, was not affected at 2 dpf (Fig. 5*D* (*lower panel*)). However, at 4 dpf, a small reduction of shortening fraction was observed in *αBb* mutants, albeit not significant, compared with WT (Fig. 5*D* (*lower panel*)). This marginally affected cardiac performance maybe offset by compensatory mechanisms, given the fact that the αB-crystallin mutants survive to adulthood.

In contrast, treatment with dexamethasone significantly reduced (~50%) the ventricular shortening fraction of the *αBb* mutants when compared with non-treated *αBb* mutants (Fig. 5*D* (*lower panel*)), whereas the heart rate of *αBb* mutants was not further affected (Fig. 5*D*). Also, compared with non-treated *αBb* mutants (Movie S1), the apparent abnormality in cardiac contraction could be observed in dexamethasone-treated *αBb* mutants (Movie S2). This result strongly highlights the contribution of αB-crystallin to the stress tolerance of the heart, in this case, for cortisol stress. Further detailed experiments are needed to examine the molecular/cellular mechanisms underlying the hypersusceptibility of cardiac tissues toward GR signaling activation in αB-crystallin mutants.

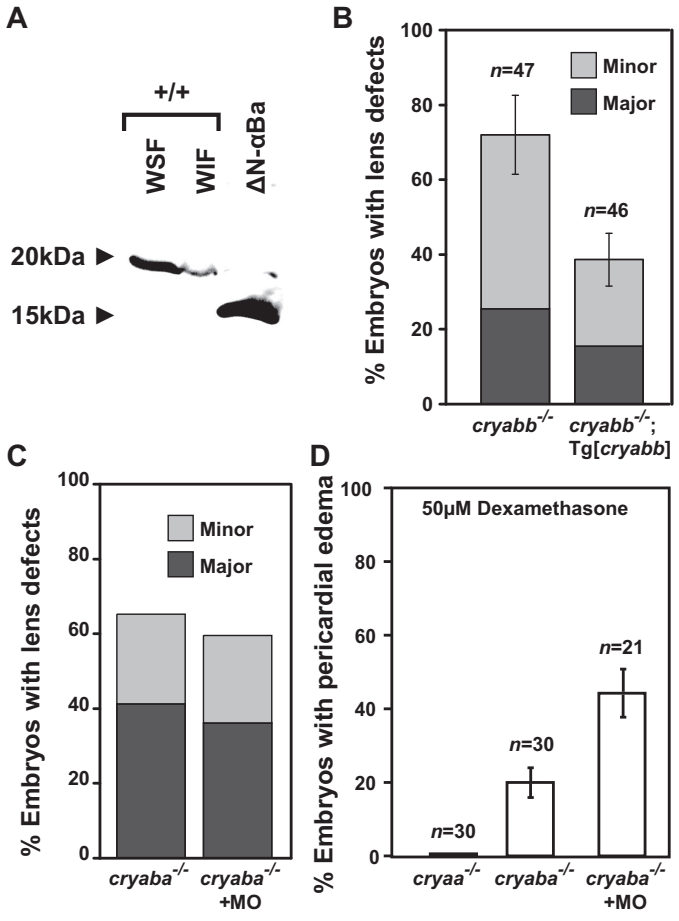

Figure 6. αB-crystallin mutations function as loss-of-function alleles. *A,* purified N-terminal truncated (Δ1–43 amino acids) αBa protein (bacterial expression) was detectable by anti-αBa polyclonal antibody. The WSF and WIF protein fractions of the excised lenses of the wild-type adult zebrafish served as control, stained for full-length αBa protein. *B,* transgenic expression of zebrafish αBb (Tg[*cryabb*]) in the lens of $\alpha Bb^{-/-}$ embryos showed suppression for its lens defects, compared with non-transgenic siblings ($\alpha Bb^{-/-}$). *C,* percentage of embryos with lens defects remained unchanged in $\alpha Ba^{-/-}$ embryos injected a morpholino (*MO*) interfering with the alternative start site compared with control $\alpha Ba^{-/-}$ embryos. *D,* GR activation-induced (50 μM dexamethasone) pericardial edema in $\alpha Ba^{-/-}$ embryos was not suppressed by injecting morpholino interfering with the alternative start site. In addition, $\alpha A^{-/-}$ embryos showed no heart edema when treated with dexamethasone.

Phenotypes of αB-crystallin mutants result from haploinsufficiency instead of a toxic gain-of-function effect

The lack of NMD and the persistent mRNA (Fig. 2*B*) described above raised a concern that the observed lens and heart defects in αB-crystallin mutants could be due to the dominant (or toxic) effects (*i.e.* gain-of-function) of residual N-terminal truncated αB-crystallin protein possibly resulting from an alternative translation even though such a possible N-terminal truncated (Δ1–43 amino acids) mutant αBa protein should be detectable by our anti-αBa antibody (Fig. 6*A*). To further exclude this possibility, we injected a morpholino specifically targeting a possible alternative initiation site into αBa mutants and examined whether the phenotypes could be suppressed. As shown in Fig. 6, *C* and *D*, there was no suppression of lens and heart phenotypes by morpholino knockdown, which argued against the αBa mutant allele functioning as dominant-negative alleles. Finally, lens-specific expression of zebrafish αBb (Tg[*cryabb*]) also partially alleviated the lens defects of αBb mutant embryos (Fig. 6*B*), which further supports the loss-of-function and haploinsufficient nature of our αB-crystallin mutant alleles.

Discussion

αB-crystallin loss-of-function mutants reveal important physiological roles

To our knowledge, this study reports the first αB-crystallin-specific loss-of-function lines in vertebrate animals. The previously described αB-crystallin knock-out mouse was in fact a compounded mutant line that also contained disruptions in the adjacent *Hspb2* gene (34) precluding a direct assessment of an exclusively αB-crystallin loss-of-function phenotype. The availability of the zebrafish model yielded novel insights into the role of αB-crystallin in the lens and cardiac muscle. Although there has been evidence of transcriptional control by the glucocorticoid receptor (58–60), our results tie this observation to a prominent role of αB-crystallin in the heart resistance to stress.

Unexpectedly, results from qRT-PCR suggested that the mRNAs encoded by the *αB* mutant alleles did not undergo significant NMD despite premature stop codons introduced in the first exons. This phenomenon of escaping NMD has been observed previously in first exon mutations (61, 62), which underscores the importance of selecting mutation target sites and confirming the mutations given the explosion of CRISPR/Cas9 genome-editing techniques (63). Several lines of evidence support our contention that the *αB* alleles described in this study function as null alleles or at least strong hypomorphic alleles, including the lack of stably expressed αBa protein as revealed by Western blot analysis (Fig. 1*C*) and quantitative proteomics by mass spectrometry (Fig. 1*D*) of homozygous mutants ($\alpha Ba^{-/-}$, $\alpha Bb^{-/-}$, and $\alpha Ba^{-/-};\alpha Bb^{-/-}$) lenses. Although it remains theoretically possible that an N-terminal truncated Cryab protein encoded by alternative downstream initiation sites contributes to the phenotype and functions as antimorphic (or neomorphic) dominant alleles (*i.e.* gain-of-function), we confidently discount this possibility not only because the N terminus of αB-crystallin has been demonstrated critical for the oligomerization and its chaperone activity (23, 64–66), but also based on the data from the alternative-translation blocking morpholino (Fig. 6, *C* and *D*), as well as the rescue of lens defects by lens-specific expression of αBb (Fig. 6*B*). Moreover, by Western analysis we were able to detect the purified N-terminal truncated mutant αBa protein that expressed in the bacterial system (Fig. 6*A*), which suggests that in *αBa* mutants the amount of the alternatively translated αBa protein, if does exist, would be negligible (Fig. 1*C*).

Unlike the lens in the mouse model (34), proper formation of embryonic lens in zebrafish shows a dosage dependence on αB-crystallin. Homozygous mutants of *αBa* and/or *αBb* develop lens abnormalities in the majority of the embryos, whereas heterozygous *αBa* and *αBb* mutants also showed lens defects albeit to a lesser extent (Fig. 3). Furthermore, consistent with an elevated *in vitro* chaperone-like activity (67), we found that *αBa* plays a more critical role in the maintenance of lens

transparency compared with *αBb* (Fig. 3). Similar to what we observed in αA-crystallin knock-out mutants (43), this gene dosage effect (or haploinsufficiency) in αB-crystallin mutants may likely reflect the low abundance of overall α-crystallin proteins in the zebrafish embryonic lens, where a small change in the expression could cause a strong response in the proteostatic network. Although not frequently reported, cataract formation could be caused by haploinsufficiency, such as mutations in *SLC16A12, PITX3*, and *PAX6* genes (68–70).

In contrast to previous reports (71–73), we detected low-level expression of *αBa* and *αBb* in the lens and the heart during zebrafish embryogenesis (Fig. 2) (43, 74). Furthermore, we found no evidence of compromised skeletal muscle functions in both αB-crystallin mutants, unlike the severe muscular phenotypes shown in a previous study using morpholino knockdown strategies (48). In addition to the notorious off-target effects of morpholino usage, it is also likely that other members of sHSP genes expressed in the myotomes, such as *hspb1*, *hspb7*, *hspb8,* and *hspb9* (73, 75), can compensate for the loss of both αB-crystallin genes and maintain a functional proteostasis network in the muscle.

Cardiac phenotypes in zebrafish αB-crystallin mutant embryos

Given the convincing literature supporting the contribution of αB-crystallin to cardiac function, particularly the genetic evidence linking an R120G mutation in αB-crystallin (CRYAB R120G) to human desmin-related cardiomyopathy (17) as well as a novel cardiomyopathy-associated CRYAB mutation, D109H (76), the lack of apparent phenotypes in the developing hearts of αB-crystallin homozygous mutants, including $\alpha Ba^{-/-}$; $\alpha Bb^{-/-}$ double mutants, was unexpected. However, the full effect of αB-crystallin deficiency may be masked or compensated by several sHSP chaperones that are robustly expressed in the developing heart tubes, such as the *hspb1*, *hspb7,* and *hspb12* (73, 75).

A major finding of this paper is the emergent role of αB-crystallin under stress conditions. αB-crystallin mutants raised under crowding stress developed severe pericardial edema in a fraction of mutant embryos, even though the penetrance was low compared with the lens phenotypes (about 10–20%; Fig. 4*B*). Interestingly, a difference in sensitivity to loss of αBa and αBb was also observed in the heart that is opposite to the lens phenotype (Fig. 3*B*). This may be a consequence of the higher level of αBb compared with αBa in the cardiomyocytes at 4-dpf embryos (77). Although we did detect expression of both αB-crystallin genes in the heart of 2-dpf embryos, the non-quantitative nature of the WMISH procedure precluded us from comparing the relative expression level between *αBa* and *αBb* genes. Additionally, differential substrate specificity or different post-translational modification of the two αB-crystallin paralogs may contribute to the variation of the gene dosage requirement in these tissues.

Similar to the lens phenotype, the cardiac phenotype does not appear to be due to a failure of specification of the cardiac tissue as both atrial and ventricular markers are normally expressed. In the non-stressed αB-crystallin mutants, we did observe a small decline of cardiac function such as slower heart rates (Fig. 5*D*). Given the known association of αB-crystallin with Desmin or Titin (10–12), subtle changes may exist at the cellular level such as sarcomere integrity, which requires further detailed analyses. Our current hypothesis is that loss of αB-crystallin would only slightly weaken the myocardium but not enough to cause severe damages (*i.e.* become sensitized); however, exposure of excess stress (*i.e.* GR agonists here) would exacerbate the phenotypes and lead to cardiac dysfunction, which is strongly supported by our observation (Fig. 5*D*).

Stress-induced phenotypes in αB-crystallin mutants uncover a novel intersection between steroid signaling and proteostasis

Following up on the established link between crowding stress and activation of glucocorticoid signaling (54, 55), we determined that the αB-crystallin mutants were highly sensitive to the treatment of GR signaling agonists, dexamethasone and hydrocortisone, and prone to develop pericardial edema (Fig. 5*A*). This synergism may be explained by the transcriptional regulation by the glucocorticoid receptor of a particular proteostatic target that leads to phenotype enhancement. Although GR-mediated transcriptional activation of sHSPs, including αB-crystallin in cell culture systems, has been demonstrated (58–60), we did not detect changes in expression of *αBa* or *αBb* (by qRT-PCR; data not shown). In fact, the action of GR signaling agonists here is unlikely to be mediated through direct transcriptional activation of the αB genes as the αB protein levels in homozygote mutants would not be affected by increased αB transcripts.

Although the importance of GR signaling in cardiac function and maintenance has been repeatedly demonstrated, the exact roles remain controversial due to its intricate regulations and interactions (78–82). Here, we provide additional wrinkles to this complex signaling system in which the proteostatic state of the cells (*i.e.* loss of αB-crystallin), in this case the cardiomyocytes, may modulate the GR signaling activities and influence the cellular responses. Thus, further experiments are needed to delineate the interactions between GR signaling and αB-crystallin.

It has been well established that prolonged corticosteroid therapy is a major risk factor for the formation of steroid-induced posterior subcapsular cataracts (PSCs), which account for ~15% of all cataracts (83–87). Although the pathoetiology and the mechanism of glucocorticoid action in the lens remain unresolved (88), two main underlying mechanisms have been examined and debated: glucocorticoid-induced gene transcription events and glucocorticoid–lens protein adduct formation (88) Only steroids with glucocorticoid activity are associated with steroid-induced PSC (89), strongly suggesting involvement of the GR (90).

Our result suggests that a compromised proteostatic system in the lens may contribute to the occurrence of steroid cataracts. Indeed, the formation of PSC is quite heterogeneous, and its dose dependence on steroid use is also controversial (91–93). Thus, we propose that individual susceptibility, which reflects the difference in genetic predisposition (such as polymorphisms in αB-crystallin gene) that impacts the lens proteostatic capacity, plays a critical role in the development of PSC. Under this assumption, instead of a "determining factor," the steroid use acts as an "environmental factor" that would facili-

Table 2
Summary of αB-crystallin iTRAQ data

Animal	WSF or WIF	Protein	Normalized fold change	*p* value	Significant?[a]
cryaba$^{-/-}$	WSF	Cryaba	0.138	7.18E-13	Yes
cryaba$^{-/-}$	WSF	Cryabb	0.610	0.039	No
cryabb$^{-/-}$	WSF	Cryaba	1.200	0.027	No
cryabb$^{-/-}$	WSF	Cryabb	0.136	5E-96	Yes
cryaba$^{-/-}$; *cryabb*$^{-/-}$	WSF	Cryaba	0.166	2.24E-11	Yes
cryaba$^{-/-}$; *cryabb*$^{-/-}$	WSF	Cryabb	0.147	1.14E-12	Yes
cryaba$^{-/-}$	WIF	Cryaba	0.077	1.28E-23	Yes
cryaba$^{-/-}$	WIF	Cryabb	0.638	0.041	No
cryabb$^{-/-}$	WIF	Cryaba	0.897	0.179	No
cryabb$^{-/-}$	WIF	Cryabb	0.161	1.13E-60	Yes
cryaba$^{-/-}$; *cryabb*$^{-/-}$	WIF	Cryaba	0.130	1.31E-10	Yes
cryaba$^{-/-}$; *cryabb*$^{-/-}$	WIF	Cryabb	0.158	5.79E-9	Yes

[a] Significance based on Benjamini-Hochberg correction for multiple comparisons.

tate the PSC formation via interactions with αB-crystallin (or other resident proteostatic factors).

Given that the physiological responses of GR signaling activation are notoriously diverse and often exhibiting profound variability in specificity or sensitivity between different tissues and individuals, partly due to its heterogeneity and complex regulation (94), the novel intersection uncovered in this study between GR signaling and proteostasis in the lens and the heart is likely tissue- or context-dependent. With gene profiling studies revealing a vast array of downstream target genes of GR signaling, further experiments utilizing genetic tools in zebrafish are set up to decipher this new interaction with potentially significant clinical relevance.

Experimental procedures

Zebrafish maintenance and breeding

AB wild-type strain zebrafish (*Danio rerio*) were used. The embryos were obtained by natural spawning and raised at 28.5 °C on a 14:10 h light/dark cycle in 0.3× Danieau water containing 0.003% PTU (w/v) to prevent pigment formation. Embryos were staged according to their ages (in dpf). The following mutant and transgenic fish lines were used: *cryaa*^{vu532} (Zou *et al.* (43)); *cryaba*^{vu612} (*αBa*^{35bpDEL}); *cryabb*^{vu613} (*αBb*^{10bpDEL}); Tg(*cryaa*:*cryabb*,*myl7*:TagRFP)^{vu614Tg}; (Tg[*cryabb*]). All animal procedures were approved by the Vanderbilt University Institutional Animal Care and Use Committee.

Generation of Cryab mutants with CRISPR/Cas9 system

To establish zebrafish mutant lines of *cryaba* and *cryabb*, gRNAs targeting the first exons of *cryaba* and *cryabb* genes were designed and screened to induce indels by injection with *Cas9* mRNA in zebrafish. Several mutant lines were established using four designed gRNAs for each gene (see Table 1). Used gRNA target sequences are presented in Table S1 and the detailed protocol of mutation generation are available upon request. Each *Cryab* mutant allele was outcrossed to AB at least two generations and then in-crossed to generate homozygous mutants, which were then analyzed for their phenotypes. Every clutch was examined carefully for peculiar phenotypes as we are aware of the possibility of off-target effects. The primers used for screening and genotyping for *Cryaba* and *Cryabb* mutant alleles are listed in Tables 2 and 3.

Zebrafish transgenesis

To establish the transgenic zebrafish expressing zebrafish *cryabb* gene specifically in the lens, transgenic construct of Tg(*cryaa*:*cryabb*,*myl7*:TagRFP) was constructed by MultiSite Gateway (Invitrogen) assembly reactions using protocols established previously (Tol2kit (95)). Specifically, entry vectors, p5E-Cryaa (96) and p3E-poly(A) were assembled with pME-Cryabb and recombined into pDestTol2CR2 vector for microinjections. Tol2-mediated transgenesis was performed as described previously (Zou *et al.* (43)). At least two founder lines (F0) for each construct were screened and out-crossed to established stable F1 generations. Each F1 line was propagated and crossed with desired mutant lines.

Morpholino knockdown

Translational-blocking antisense phosphorodiamidate oligonucleotide (morpholino, MO) against the potential alternative start site of *cryaba*^{35bpDEL} allele was designed and synthesized by Gene Tools (5′-GGACGATAGTAAAACATGGTGTAGA-3′; Philomath, OR). 5 ng of MO was injected into the yolk of 1–2-cell stage zygotes, which were the progenies from *cryaba*$^{-/-}$ incross.

Crowding and drug treatments

For crowding stress, 1-dpf embryos were manually dechorined, and 75 embryos were placed in one well of a 6-well plate (polystyrene, tissue culture grade) with 5 ml of 0.3× Danieau water. For control, 15 embryos per well were used as non-stressed condition. To mimic the effect of glucocorticoid stress, we used pharmacological stimulation by treating embryos with 50 μM dexamethasone (Sigma, D1756) and 50 μM hydrocortisone (Sigma, H2270) diluted in 0.3× Danieau water (24-well plate, 10 embryos/well) from 1 until 4 dpf to examine the cardiac phenotypes. The optimal dosages of dexamethasone and hydrocortisone were determined after dose-response analysis.

Western analysis

Both lenses of each adult zebrafish (WT and *Cryab* mutants) were excised, washed, and homogenized in lysis buffer (20 mM Tris-HCl, pH 7.6, 100 mM NaCl, 1 mM NaN_3, 1 mM EDTA) (4) and supplemented with 1 mM PMSF and COmplete protease mixture (Roche Applied Science). The homogenate was centrifuged at 15,000 × *g* at 4 °C to separate water-soluble and water-

Table 3
Survival analysis of the progeny from incross of αB-crystallin heterozygotes

	Cryaba^{35bpDEL}			Cryabb^{10bpDEL}		
	Homozygote (−/−)	Heterozygote (−/+)	WT (+/+)	Homozygote (−/−)	Heterozygote (−/+)	WT (+/+)
% per genotype (expected, 25:50:25%)	24%	49%	27%	22%	51%	27%
Survival rate (%) 10 months old	96%	90%	89%	88%	86%	75%

insoluble fractions. Both fractions from each lens were heated in a water bath for 5 min after adding 2× Laemmli Sample Buffer supplemented with DTT and spun at benchtop to clear the solutions. Protein concentrations were measured by RcDc protein assay kit (Bio-Rad). 10 μg of total proteins separated by 12% SDS-PAGE were transferred to nitrocellulose membrane in Towbin buffer and probed with custom Anti-αA and Anti-αBa polyclonal antibodies (Vanderbilt Antibody and Protein Resource Core), which were generated by injecting full-length αA and αBa proteins, purified from bacterial expression system, as described previously (67), in rabbits. Antisera from two rabbits each, for both proteins, were tested for titer, and after booster shots the antibodies were affinity-purified from the final bleeds using purified proteins as antigens. The blots were visualized by anti-HRP secondary antibody (Promega) using enhanced chemiluminescence (HyGLO^{TM} Quick Spray Chemiluminescent; Denville Scientific Inc.). The cDNA construct encoding the N-terminally truncated αBa protein (Δ1–43 amino acids) was generated by PCR cloning and cloned into pET-20b(+) bacterial expression vector (Novagen).

WMISH

Linearized full-length coding sequence of *cryaba* and *cryabb*, with added T7 polymerase site, was PCR-amplified from the cDNA clones (obtained from Mason Posner (Ashland University, Ashland, OH). The digoxygenin-labeled ISH probes were generated by transcribing with T7 RNA polymerase (New England Biolabs) and DIG RNA Labeling Mix (Roche Applied Science). Subsequently, RNA probes were purified after TRIzol precipitation using Direct-zol miniprep kit (Zymo Research) and confirmed for purity and length (507 bp for *cryaba* and 498 bp for *cryabb*) by agarose gel electrophoresis. The whole-mount *in situ* hybridization on 2-dpf embryos was performed according to established protocol (44).

Quantitative RT-PCR

Total RNAs were isolated from embryos at desired stages (2- and 4-dpf) by using TRIzol reagent (Invitrogen), followed by DNase treatment (Ambion). The iScript cDNA synthesis kit (Bio-Rad) was used for reverse transcriptions, and subsequent qRT-PCRs (SsoAdvanced Universal SYBR Green Supermix, Bio-Rad) were performed on Bio-Rad CFX96 Real-Time PCR Detection System according to manufacturer's protocols (the cycling parameters were as follows: 95 °C for 10 min, 40 cycles of 95 °C for 15 s, and 60 °C for 30 s). The PCR products were analyzed by gel electrophoresis to confirm that they were of the expected size. The CFX Manager software provided with the thermocycler (Bio-Rad) was used to determine *Ct* values. Expression differences between samples were calculated by the $-\Delta\Delta Ct$ (comparative *Ct*) method and reported without log2 conversion to fold changes. Three pools of 10 embryos from separate clutches of each transgenic line were collected, and each sample was analyzed in triplicate. The primers (including β-actin as an internal control) used in this study are listed in Table S4.

Cell death assays

Embryos were fixed overnight at 4 °C in 4% paraformaldehyde in PBS, dehydrated with 100% methanol, and stored in −20 °C. The procedures of TUNEL staining were carried out following the manufacturer's suggested protocol (*In Situ* Cell Death Detection Kit, TMR red; Sigma catalog no. 12156792910).

Immunohistochemistry

Embryos were fixed overnight at 4 °C in 4% paraformaldehyde in PBS, and the anti-MF20 (ventricle) and anti-S46 (atrium) (Developmental Studies Hybridoma Bank) staining of the heart were performed as described previously (97). The secondary antibodies used were anti-IgG2b-Alexa 568 (for MF20; Invitrogen) and the anti-IgG1-Alexa 488 (for S46; Invitrogen).

Heart imaging and cardiac function measurements

Videos taken of the zebrafish hearts *in vivo* (Zeiss AxioZoomV16 microscope) were used to calculate shortening fraction (calculate the shortening fraction (%) for the ventricle as follows: 100 × (width at diastole − width at systole)/(width at diastole) and for heart rate (count the number of beats in 15 s and then multiply the number of beats counted as beats/min), following the established protocol (98).

Microscopy and image processing

Lenses of live embryos in 0.3× Daneau water with PTU/tricaine were analyzed by bright field microscopy (Zeiss Axiovert 200) at 4 dpf and graded into three classes depending on the severity of lens defects as defined in our previous study (43). Briefly, the phenotypic features appeared as either round, shiny crystal-like droplets spread across the lens that were classified as minor defects or large irregular protuberances located in the center of the lens classified as major defects. Fluorescence images were taken with Zeiss AxioZoom.V16 microscope.

iTRAQ quantification of protein changes

To quantify protein expression changes in zebrafish lenses, one lens from 6-month-old fish of each genotype (WT, *cryaba*$^{-/-}$, *cryabb*$^{-/-}$ and *cryaba*$^{-/-}$;*cryabb*$^{-/-}$) were homogenized in 50 ml of homogenizing buffer (for lens: 25 mM Tris, 150 mM NaCl, 1 mM PMSF, 5 mM EDTA, 10 mM NaF, pH 7.5). The samples were centrifuged at 20,000 × *g* for 20 min, and pellets were washed with another 50 ml of homogenizing buffer

followed by centrifugation at 20,000 × *g*. The supernatants were pooled together as the WSF. Protein concentrations for WSF fractions were measured by Bradford assay (Thermo Fisher Scientific, Rockford, IL). The pellets were considered as the WIF. WIF was washed with water twice and suspended in 100 ml of water, and an aliquot was mixed with equal volume of 5% SDS for a BCA assay (Thermo Fisher Scientific). 80 mg of WSF from each lens (and 50 mg from each heart) was reduced with 50 mM tris-(2-carboxyethyl)phosphine at 60 °C for 1 h, alkylated with 200 mM methyl methanethiosulfonate (MMTS) at room temperature for 10 min, and digested with sequencing-grade trypsin overnight. 20 μg of each WSF fraction was then labeled with iTRAQ reagents according to the manufacturer's instructions (AB Sciex, Foster City, CA) (114 for WT, 115 for *cryaba*$^{-/-}$, 116 for *cryabb*$^{-/-}$,and 117 for *cryaba*$^{-/-}$;*cryabb*$^{-/-}$). For WIF fractions, the entire reconstituted pellet for each WIF sample was digested with trypsin, and 18 μg was labeled with iTRAQ reagents. Reagents were reconstituted in ethanol such that each protein sample was iTRAQ-labeled at a final concentration of 90% ethanol, and labeling was performed for 2 h.

The iTRAQ-labeled samples were mixed, acidified with TFA, and subsequently desalted by a modified Stage-tip method prior to LC-MS/MS analysis. iTRAQ-labeled samples were analyzed using MudPIT analysis with 13 salt pulse steps (0, 25, 50, 75, 100, 150, 200, 250, 300, and 500 mM and 1 and 2 M ammonium acetate). Peptides were introduced via nano-electrospray into a Q Exactive HF mass spectrometer (Thermo Fisher Scientific, San Jose, CA). The Q Exactive was operated in data-dependent mode acquiring HCD MS/MS scans (R = 15,000) after each MS1 scan (R = 60,000) on the 15 most abundant ions using an MS1 ion target of 3×10^6 ions and an MS2 target of 1×10^5 ions. The HCD-normalized collision energy was set to 30, dynamic exclusion was set to 30 s, and peptide match and isotope exclusion were enabled. For iTRAQ data analysis, mass spectra were processed using the Spectrum Mill software package (version B.04.00, Agilent Technologies). MS/MS spectra acquired on the same precursor m/z (±0.01 m/z) within ±1 s in retention time were merged. MS/MS spectra of poor quality, which failed the quality filter by not having a sequence tag length of >1, were excluded from searching. A minimum matched peak intensity requirement was set to 50%. For peptide identification, MS/MS spectra were searched against a Uniprot zebrafish database (June 21, 2012). Additional search parameters included the following: trypsin enzyme specificity with a maximum of three missed cleavages; ±20 ppm precursor mass tolerance; ±20 ppm (HCD) product mass tolerance; and fixed modifications including MMTS alkylation of cysteines and iTRAQ labeling of lysines and peptide N termini. Oxidation of methionine was allowed as a variable modification. Autovalidation was performed such that peptide assignments to mass spectra were designated as valid following an automated procedure during which score thresholds were optimized separately for each precursor charge state, and the maximum target-decoy-based false-discovery rate was set to 1.0% (99).

Statistics

Differences among groups were analyzed by Student's t test. Data are shown as means ± S.E. Statistical significance was accepted when $p < 0.05$.

For statistical analysis of iTRAQ protein ratios, $\log_2$ protein ratios were fit to normal distribution using non-linear (least squares) regression. The mean and standard deviation values derived from the Gaussian fit were used to calculate p values, using Z score statistics. A given $\log_2$ iTRAQ protein ratio (x), with the calculated mean (μ) and standard deviation of the fitted data (σ), was transformed to a standard normal variable ($z = (x - \mu/\sigma)$. Calculated p values were subsequently corrected for multiple comparisons using the Benjamini-Hochberg method (100).

Author contributions—S. M. and S.-Y. W. contributed to conception of the research, designed and performed the research, analyzed the data, and wrote the paper. A. W. F. performed the research and analyzed the data. Z. W., K. L. R., and K. L. S. performed the research, analyzed the data, and wrote part of the paper. H. S. M. contributed to conception of the research, designed the research and wrote the paper. All authors reviewed the results and approved the final version of the manuscript.

Acknowledgments—We thank Drs. Derek Claxton and Richard Stein for critical reading of the manuscript and Dr. Wenbiao Chen for technical assistance. We are grateful for Dr. Patrick Page-McCaw for thoughtful discussions, insights, and detailed editing of the manuscript.

References

1. Boelens, W. C. (2014) Cell biological roles of αB-crystallin. *Prog. Biophys. Mol. Biol.* **115,** 3–10 CrossRef Medline
2. Arrigo, A. P., Simon, S., Gibert, B., Kretz-Remy, C., Nivon, M., Czekalla, A., Guillet, D., Moulin, M., Diaz-Latoud, C., and Vicart, P. (2007) Hsp27 (HspB1) and αB-crystallin (HspB5) as therapeutic targets. *FEBS Lett.* **581,** 3665–3674 CrossRef Medline
3. Akerfelt, M., Morimoto, R. I., and Sistonen, L. (2010) Heat shock factors: integrators of cell stress, development and lifespan. *Nat. Rev. Mol. Cell Biol.* **11,** 545–555 CrossRef Medline
4. Horwitz, J. (1992) α-Crystallin can function as a molecular chaperone. *Proc. Natl. Acad. Sci. U.S.A.* **89,** 10449–10453 CrossRef Medline
5. Jakob, U., Gaestel, M., Engel, K., and Buchner, J. (1993) Small heat shock proteins are molecular chaperones. *J. Biol. Chem.* **268,** 1517–1520 Medline
6. Muchowski, P. J., Bassuk, J. A., Lubsen, N. H., and Clark, J. I. (1997) Human αB-crystallin. Small heat shock protein and molecular chaperone. *J. Biol. Chem.* **272,** 2578–2582 CrossRef Medline
7. Koteiche, H. A., and McHaourab, H. S. (2003) Mechanism of chaperone function in small heat-shock proteins. Phosphorylation-induced activation of two-mode binding in αB-crystallin. *J. Biol. Chem.* **278,** 10361–10367 CrossRef Medline
8. Reddy, V. S., and Reddy, G. B. (2015) Emerging role for αB-crystallin as a therapeutic agent: pros and cons. *Curr. Mol. Med.* **15,** 47–61 CrossRef Medline
9. Mymrikov, E. V., Daake, M., Richter, B., Haslbeck, M., and Buchner, J. (2017) The chaperone activity and substrate spectrum of human small heat shock proteins. *J. Biol. Chem.* **292,** 672–684 CrossRef Medline
10. Bullard, B., Ferguson, C., Minajeva, A., Leake, M. C., Gautel, M., Labeit, D., Ding, L., Labeit, S., Horwitz, J., Leonard, K. R., and Linke, W. A. (2004) Association of the chaperone αB-crystallin with titin in heart muscle. *J. Biol. Chem.* **279,** 7917–7924 CrossRef Medline

11. Bennardini, F., Wrzosek, A., and Chiesi, M. (1992) αB-crystallin in cardiac tissue. Association with actin and desmin filaments. *Circ. Res.* **71,** 288–294 CrossRef Medline
12. Perng, M. D., Muchowski, P. J., van den IJssel, P., Wu, G. J. S., Hutcheson, A. M., Clark J. I., and Quinlan, R. A. (1999) The cardiomyopathy and lens cataract mutation in αB-crystallin compromises secondary, tertiary and quaternary protein structure and reduces *in vitro* chaperone activity. *J. Biol. Chem.* **274,** 33235–33243 CrossRef Medline
13. Neppl, R. L., Kataoka, M., and Wang, D. Z. (2014) Crystallin-αB regulates skeletal muscle homeostasis via modulation of argonaute2 activity. *J. Biol. Chem.* **289,** 17240–17248 CrossRef Medline
14. Selcen, D., and Engel, A. G. (2003) Myofibrillar myopathy caused by novel dominant negative αB-crystallin mutations. *Ann. Neurol.* **54,** 804–810 CrossRef Medline
15. Simon, S., Fontaine, J. M., Martin, J. L., Sun, X., Hoppe, A. D., Welsh, M. J., Benndorf, R., and Vicart, P. (2007) Myopathy-associated αB-crystallin mutants: abnormal phosphorylation, intracellular location, and interactions with other small heat shock proteins. *J. Biol. Chem.* **282,** 34276–34287 CrossRef Medline
16. Forrest, K. M., Al-Sarraj, S., Sewry, C., Buk, S., Tan, S. V., Pitt, M., Durward, A., McDougall, M., Irving, M., Hanna, M. G., Matthews, E., Sarkozy, A., Hudson, J., Barresi, R., Bushby, K., *et al.* (2011) Infantile onset myofibrillar myopathy due to recessive CRYAB mutations. *Neuromuscul. Disord.* **21,** 37–40 CrossRef Medline
17. Vicart, P., Caron, A., Guicheney, P., Li, Z., Prévost, M. C., Faure, A., Chateau, D., Chapon, F., Tomé, F., Dupret, J. M., Paulin, D., and Fardeau, M. (1998) A missense mutation in the αB-crystallin chaperone gene causes a desmin-related myopathy. *Nat. Genet.* **20,** 92–95 CrossRef Medline
18. Sharma, K. K., Kaur, H., and Kester, K. (1997) Functional elements in molecular chaperone α-crystallin: identification of binding sites in αB-crystallin. *Biochem. Biophys. Res. Commun.* **239,** 217–222 CrossRef Medline
19. Ghosh, J. G., Shenoy, A. K., Jr., and Clark, J. I. (2006) N- and C-terminal motifs in human αB crystallin play an important role in the recognition, selection, and solubilization of substrates. *Biochemistry* **45,** 13847–13854 CrossRef Medline
20. Bhattacharyya, J., Padmanabha Udupa, E. G., Wang, J., and Sharma, K. K. (2006) Mini-αB-crystallin: a functional element of αB-crystallin with chaperone-like activity. *Biochemistry* **45,** 3069–3076 CrossRef Medline
21. McHaourab, H. S., Godar, J. A., and Stewart, P. L. (2009) Structure and mechanism of protein stability sensors: chaperone activity of small heat shock proteins. *Biochemistry* **48,** 3828–3837 CrossRef Medline
22. Ghosh, J. G., and Clark, J. I. (2005) Insights into the domains required for dimerization and assembly of human αB crystallin. *Protein Sci.* **14,** 684–695 CrossRef Medline
23. Jehle, S., Vollmar, B. S., Bardiaux, B., Dove, K. K., Rajagopal, P., Gonen, T., Oschkinat, H., and Klevit, R. E. (2011) N-terminal domain of αB-crystallin provides a conformational switch for multimerization and structural heterogeneity. *Proc. Natl. Acad. Sci. U.S.A.* **108,** 6409–6414 CrossRef Medline
24. Delbecq, S. P., Rosenbaum, J. C., and Klevit, R. E. (2015) A mechanism of subunit recruitment in human small heat shock protein oligomers. *Biochemistry* **54,** 4276–4284 CrossRef Medline
25. Basha, E., O'Neill, H., and Vierling, E. (2012) Small heat shock proteins and α-crystallins: dynamic proteins with flexible functions. *Trends Biochem. Sci.* **37,** 106–117 CrossRef Medline
26. Koteiche, H. A., and Mchaourab, H. S. (2006) Mechanism of a hereditary cataract phenotype. Mutations in αA-crystallin activate substrate binding. *J. Biol. Chem.* **281,** 14273–14279 CrossRef Medline
27. Shi, J., Koteiche, H. A., McDonald, E. T., Fox, T. L., Stewart, P. L., and McHaourab, H. S. (2013) Cryoelectron microscopy analysis of small heat shock protein 16.5 (Hsp16.5) complexes with T4 lysozyme reveals the structural basis of multimode binding. *J. Biol. Chem.* **288,** 4819–4830 CrossRef Medline
28. Shi, J., Koteiche, H. A., McHaourab, H. S., and Stewart, P. L. (2006) Cryoelectron microscopy and EPR analysis of engineered symmetric and polydisperse Hsp16.5 assemblies reveals determinants of polydispersity and substrate binding. *J. Biol. Chem.* **281,** 40420–40428 CrossRef Medline
29. McHaourab, H. S., Lin, Y. L., and Spiller, B. W. (2012) Crystal structure of an activated variant of small heat shock protein Hsp16.5. *Biochemistry* **51,** 5105–5112 CrossRef Medline
30. Shashidharamurthy, R., Koteiche, H. A., Dong, J., and McHaourab, H. S. (2005) Mechanism of chaperone function in small heat shock proteins: dissociation of the HSP27 oligomer is required for recognition and binding of destabilized T4 lysozyme. *J. Biol. Chem.* **280,** 5281–5289 CrossRef Medline
31. Peschek, J., Braun, N., Rohrberg, J., Back, K. C., Kriehuber, T., Kastenmüller, A., Weinkauf, S., and Buchner, J. (2013) Regulated structural transitions unleash the chaperone activity of αB-crystallin. *Proc. Natl. Acad. Sci. U.S.A.* **110,** E3780–E3789 CrossRef Medline
32. Thornell, E., and Aquilina, A. (2015) Regulation of αA- and αB-crystallins via phosphorylation in cellular homeostasis. *Cell. Mol. Life Sci.* **72,** 4127–4137 CrossRef Medline
33. Bakthisaran, R., Akula, K. K., Tangirala, R., and Rao, Ch. M. (2016) Phosphorylation of αB-crystallin: role in stress, aging and patho-physiological conditions. *Biochim. Biophys. Acta* **1860,** 167–182 CrossRef Medline
34. Brady, J. P., Garland, D. L., Green, D. E., Tamm, E. R., Giblin, F. J., and Wawrousek, E. F. (2001) αB-crystallin in lens development and muscle integrity: a gene knockout approach. *Invest. Ophthalmol. Vis. Sci.* **42,** 2924–2934 Medline
35. Pinz, I., Robbins, J., Rajasekaran, N. S., Benjamin, I. J., and Ingwall, J. S. (2008) Unmasking different mechanical and energetic roles for the small heat shock proteins CryAB and HSPB2 using genetically modified mouse hearts. *FASEB J.* **22,** 84–92 Medline
36. Benjamin, I. J., Guo, Y., Srinivasan, S., Boudina, S., Taylor, R. P., Rajasekaran, N. S., Gottlieb, R., Wawrousek, E. F., Abel, E. D., and Bolli, R. (2007) CRYAB and HSPB2 deficiency alters cardiac metabolism and paradoxically confers protection against myocardial ischemia in aging mice. *Am. J. Physiol. Heart Circ. Physiol.* **293,** H3201–H3209 CrossRef Medline
37. Hwang, W. Y., Fu, Y., Reyon, D., Maeder, M. L., Tsai, S. Q., Sander, J. D., Peterson, R. T., Yeh, J. R., and Joung, J. K. (2013) Efficient genome editing in zebrafish using a CRISPR-Cas system. *Nat. Biotechnol.* **31,** 227–229 CrossRef Medline
38. Jao, L. E., Wente, S. R., and Chen, W. (2013) Efficient multiplex biallelic zebrafish genome editing using a CRISPR nuclease system. *Proc. Natl. Acad. Sci. U.S.A.* **110,** 13904–13909 CrossRef Medline
39. Jinek, M., Chylinski, K., Fonfara, I., Hauer, M., Doudna, J. A., and Charpentier, E. (2012) A programmable dual-RNA-guided DNA endonuclease in adaptive bacterial immunity. *Science* **337,** 816–821 CrossRef Medline
40. Wang, Z., and Schey, K. L. (2015) Proteomic analysis of lipid raft-like detergent-resistant membranes of lens fiber cells. *Invest. Ophthalmol. Vis. Sci.* **56,** 8349–8360 CrossRef Medline
41. Nahomi, R. B., Huang, R., Nandi, S. K., Wang, B., Padmanabha, S., Santhoshkumar, P., Filipek, S., Biswas, A., and Nagaraj, R. H. (2013) Acetylation of lysine 92 improves the chaperone and anti-apoptotic activities of human αB-crystallin. *Biochemistry* **52,** 8126–8138 CrossRef Medline
42. Krishnamoorthy, V., Donofrio, A. J., and Martin, J. L. (2013) *O*-GlcNAcylation of αB-crystallin regulates its stress-induced translocation and cytoprotection. *Mol. Cell. Biochem.* **379,** 59–68 CrossRef Medline
43. Zou, P., Wu, S. Y., Koteiche, H. A., Mishra, S., Levic, D. S., Knapik, E., Chen, W., and Mchaourab, H. S. (2015) A conserved role of αA-crystallin in the development of the zebrafish embryonic lens. *Exp. Eye Res.* **138,** 104–113 CrossRef Medline
44. Thisse, B., and Thisse, C. (2014) *In situ* hybridization on whole-mount zebrafish embryos and young larvae. *Methods Mol. Biol.* **1211,** 53–67 CrossRef Medline
45. Li, J., Yuan, Z., and Zhang, Z. (2010) The cellular robustness by genetic redundancy in budding yeast. *PLoS Genet.* **6,** e1001187 CrossRef Medline
46. Davidson, E. H., Rast, J. P., Oliveri, P., Ransick, A., Calestani, C., Yuh, C. H., Minokawa, T., Amore, G., Hinman, V., Arenas-Mena, C., Otim, O., Brown, C. T., Livi, C. B., Lee, P. Y., Revilla, R., *et al.* (2002) A provisional regulatory gene network for specification of endomesoderm in the sea

urchin embryo. *Dev. Biol.* **246,** 162–190 CrossRef Medline
47. Inagaki, N., Hayashi, T., Arimura, T., Koga, Y., Takahashi, M., Shibata, H., Teraoka, K., Chikamori, T., Yamashina, A., and Kimura, A. (2006) αB-crystallin mutation in dilated cardiomyopathy. *Biochem. Biophys. Res. Commun.* **342,** 379–386 CrossRef Medline
48. Bührdel, J. B., Hirth, S., Kessler, M., Westphal, S., Forster, M., Manta, L., Wiche, G., Schoser, B., Schessl, J., Schröder, R., Clemen, C. S., Eichinger, L., Fürst, D. O., van der Ven, P. F., Rottbauer, W., and Just, S. (2015) *In vivo* characterization of human myofibrillar myopathy genes in zebrafish. *Biochem. Biophys. Res. Commun.* **461,** 217–223 CrossRef Medline
49. Kok, F. O., Shin, M., Ni, C. W., Gupta, A., Grosse, A. S., van Impel, A., Kirchmaier, B. C., Peterson-Maduro, J., Kourkoulis, G., Male, I., DeSantis, D. F., Sheppard-Tindell, S., Ebarasi, L., Betsholtz, C., Schulte-Merker, S., *et al.* (2015) Reverse genetic screening reveals poor correlation between morpholino-induced and mutant phenotypes in zebrafish. *Dev. Cell* **32,** 97–108 CrossRef Medline
50. Head, M. W., Corbin, E., and Goldman, J. E. (1994) Coordinate and independent regulation of αB-crystallin and hsp27 expression in response to physiological stress. *J. Cell. Physiol.* **159,** 41–50 CrossRef Medline
51. Ito, H., Okamoto, K., Nakayama, H., Isobe, T., and Kato, K. (1997) Phosphorylation of αB-crystallin in response to various types of stress. *J. Biol. Chem.* **272,** 29934–29941 CrossRef Medline
52. Djabali, K., de Néchaud, B., Landon, F., and Portier, M. M. (1997) αB-crystallin interacts with intermediate filaments in response to stress. *J. Cell Sci.* **110,** 2759–2769 Medline
53. Xu, X., Meiler, S. E., Zhong, T. P., Mohideen, M., Crossley, D. A., Burggren, W. W., and Fishman, M. C. (2002) Cardiomyopathy in zebrafish due to mutation in an alternatively spliced exon of titin. *Nat. Genet.* **30,** 205–209 Medline
54. Ramsay, J. M., Feist, G. W., Varga, Z. M., Westerfield, M., Kent, M. L., and Schreck, C. B. (2006) Whole-body cortisol is an indicator of crowding stress in adult zebrafish, *Danio rerio*. *Aquaculture* **258,** 565–574 CrossRef
55. Sallin, P., and Jazwinska, A. (2016) Acute stress is detrimental to heart regeneration in zebrafish. *Open Biol.* **6,** 160012 CrossRef Medline
56. Chen, Q., Jia, A., Snyder, S. A., Gong, Z., and Lam, S. H. (2016) Glucocorticoid activity detected by *in vivo* zebrafish assay and *in vitro* glucocorticoid receptor bioassay at environmental relevant concentrations. *Chemosphere* **144,** 1162–1169 CrossRef Medline
57. Nesan, D., and Vijayan, M. M. (2012) Embryo exposure to elevated cortisol level leads to cardiac performance dysfunction in zebrafish. *Mol. Cell. Endocrinol.* **363,** 85–91 CrossRef Medline
58. Aoyama, A., Fröhli, E., Schäfer, R., and Klemenz, R. (1993) αB-crystallin expression in mouse NIH 3T3 fibroblasts: glucocorticoid responsiveness and involvement in thermal protection. *Mol. Cell. Biol.* **13,** 1824–1835 CrossRef Medline
59. Kinyamu, H. K., Collins, J. B., Grissom, S. F., Hebbar, P. B., and Archer, T. K. (2008) Genome wide transcriptional profiling in breast cancer cells reveals distinct changes in hormone receptor target genes and chromatin modifying enzymes after proteasome inhibition. *Mol. Carcinog.* **47,** 845–885 CrossRef Medline
60. Cheng, X., Zhao, X., Khurana, S., Bruggeman, L. A., and Kao, H. Y. (2013) Microarray analyses of glucocorticoid and vitamin D3 target genes in differentiating cultured human podocytes. *PLoS One* **8,** e60213 CrossRef Medline
61. Neu-Yilik, G., Amthor, B., Gehring, N. H., Bahri, S., Paidassi, H., Hentze, M. W., and Kulozik, A. E. (2011) Mechanism of escape from nonsense-mediated mRNA decay of human β-globin transcripts with nonsense mutations in the first exon. *RNA* **17,** 843–854 CrossRef Medline
62. Cain, J. T., Kim, D. I., Quast, M., Shivega, W. G., Patrick, R. J., Moser, C., Reuter, S., Perez, M., Myers, A., Weimer, J. M., Roux, K. J., and Landsverk, M. (2017) Nonsense pathogenic variants in exon 1 of PHOX2B lead to translational reinitiation in congenital central hypoventilation syndrome. *Am. J. Med. Genet. A* **173,** 1200–1207 CrossRef Medline
63. Mou, H., Smith, J. L., Peng, L., Yin, H., Moore, J., Zhang, X. O., Song, C. Q., Sheel, A., Wu, Q., Ozata, D. M., Li, Y., Anderson, D. G., Emerson, C. P., Sontheimer, E. J., Moore, M. J., *et al.* (2017) CRISPR/Cas9-mediated genome editing induces exon skipping by alternative splicing or exon deletion. *Genome Biol.* **18,** 108 CrossRef Medline
64. Bova, M. P., McHaourab, H. S., Han, Y., and Fung, B. K. (2000) Subunit exchange of small heat shock proteins. Analysis of oligomer formation of αA-crystallin and Hsp27 by fluorescence resonance energy transfer and site-directed truncations. *J. Biol. Chem.* **275,** 1035–1042 CrossRef Medline
65. Santhoshkumar, P., Murugesan, R., and Sharma, K. K. (2009) Deletion of (54)FLRAPSWF(61) residues decreases the oligomeric size and enhances the chaperone function of αB-crystallin. *Biochemistry* **48,** 5066–5073 CrossRef Medline
66. Asomugha, C. O., Gupta, R., and Srivastava, O. P. (2011) Structural and functional properties of NH(2)-terminal domain, core domain, and COOH-terminal extension of αA- and αB-crystallins. *Mol. Vis.* **17,** 2356–2367 Medline
67. Koteiche, H. A., Claxton, D. P., Mishra, S., Stein, R. A., McDonald, E. T., and Mchaourab, H. S. (2015) Species-specific structural and functional divergence of α-crystallins: zebrafish αBa- and rodent αA(ins)-crystallin encode activated chaperones. *Biochemistry* **54,** 5949–5958 CrossRef Medline
68. Castorino, J. J., Gallagher-Colombo, S. M., Levin, A. V., Fitzgerald, P. G., Polishook, J., Kloeckener-Gruissem, B., Ostertag, E., and Philp, N. J. (2011) Juvenile cataract-associated mutation of solute carrier SLC16A12 impairs trafficking of the protein to the plasma membrane. *Invest. Ophthalmol. Vis. Sci.* **52,** 6774–6784 CrossRef Medline
69. Bidinost, C., Matsumoto, M., Chung, D., Salem, N., Zhang, K., Stockton, D. W., Khoury, A., Megarbane, A., Bejjani, B. A., and Traboulsi, E. I. (2006) Heterozygous and homozygous mutations in PITX3 in a large Lebanese family with posterior polar cataracts and neurodevelopmental abnormalities. *Invest. Ophthalmol. Vis. Sci.* **47,** 1274–1280 CrossRef Medline
70. Glaser, T., Jepeal, L., Edwards, J. G., Young, S. R., Favor, J., and Maas, R. L. (1994) PAX6 gene dosage effect in a family with congenital cataracts, aniridia, anophthalmia and central nervous system defects. *Nat. Genet.* **7,** 463–471 CrossRef Medline
71. Posner, M., Kantorow, M., and Horwitz, J. (1999) Cloning, sequencing and differential expression of αB-crystallin in the zebrafish, *Danio rerio*. *Biochim. Biophys. Acta* **1447,** 271–277 CrossRef Medline
72. Elicker, K. S., and Hutson, L. D. (2007) Genome-wide analysis and expression profiling of the small heat shock proteins in zebrafish. *Gene* **403,** 60–69 CrossRef Medline
73. Marvin, M., O'Rourke, D., Kurihara, T., Juliano, C. E., Harrison, K. L., and Hutson, L. D. (2008) Developmental expression patterns of the zebrafish small heat shock proteins. *Dev. Dyn.* **237,** 454–463 CrossRef Medline
74. Harding, R. L., Howley, S., Baker, L. J., Murphy, T. R., Archer, W. E., Wistow, G., Hyde, D. R., and Vihtelic, T. S. (2008) Lengsin expression and function during zebrafish lens formation. *Exp. Eye Res.* **86,** 807–818 CrossRef Medline
75. Mao, L., and Shelden, E. A. (2006) Developmentally regulated gene expression of the small heat shock protein Hsp27 in zebrafish embryos. *Gene Expr. Patterns* **6,** 127–133 CrossRef Medline
76. Sacconi, S., Féasson, L., Antoine, J. C., Pécheux, C., Bernard, R., Cobo, A. M., Casarin, A., Salviati, L., Desnuelle, C., and Urtizberea, A. (2012) A novel CRYAB mutation resulting in multisystemic disease. *Neuromuscul. Disord.* **22,** 66–72 CrossRef Medline
77. Shih, Y. H., Zhang, Y., Ding, Y., Ross, C. A., Li, H., Olson, T. M., and Xu, X. (2015) Cardiac transcriptome and dilated cardiomyopathy genes in zebrafish. *Circ. Cardiovasc. Genet.* **8,** 261–269 CrossRef Medline
78. Rog-Zielinska, E. A., Richardson, R. V., Denvir, M. A., and Chapman, K. E. (2014) Glucocorticoids and foetal heart maturation; implications for prematurity and foetal programming. *J. Mol. Endocrinol.* **52,** R125–R135 CrossRef Medline
79. Roy, S. G., De, P., Mukherjee, D., Chander, V., Konar, A., Bandyopadhyay, D., and Bandyopadhyay, A. (2009) Excess of glucocorticoid induces cardiac dysfunction via activating angiotensin II pathway. *Cell. Physiol. Biochem.* **24,** 1–10 CrossRef Medline
80. Sainte-Marie, Y., Nguyen Dinh Cat, A., Perrier, R., Mangin, L., Soukaseum, C., Peuchmaur, M., Tronche, F., Farman, N., Escoubet, B., Benitah,

J. P., and Jaisser, F. (2007) Conditional glucocorticoid receptor expression in the heart induces atrio-ventricular block. *FASEB J.* **21,** 3133–3141 CrossRef Medline
81. Oakley, R. H., and Cidlowski, J. A. (2015) Glucocorticoid signaling in the heart: a cardiomyocyte perspective. *J. Steroid Biochem. Mol. Biol.* **153,** 27–34 CrossRef Medline
82. Oakley, R. H., Ren, R., Cruz-Topete, D., Bird, G. S., Myers, P. H., Boyle, M. C., Schneider, M. D., Willis, M. S., and Cidlowski, J. A. (2013) Essential role of stress hormone signaling in cardiomyocytes for the prevention of heart disease. *Proc. Natl. Acad. Sci. U.S.A.* **110,** 17035–17040 CrossRef Medline
83. Leske, M. C., Chylack, L. T., Jr., He, Q., Wu, S. Y., Schoenfeld, E., Friend, J., and Wolfe, J. (1997) Incidence and progression of cortical and posterior subcapsular opacities: the Longitudinal Study of Cataract. The LSC Group. *Ophthalmology* **104,** 1987–1993 CrossRef Medline
84. McCarty, C. A., Nanjan, M. B., and Taylor, H. R. (2000) Attributable risk estimates for cataract to prioritize medical and public health action. *Invest. Ophthalmol. Vis. Sci.* **41,** 3720–3725 Medline
85. Renfro, L., and Snow, J. S. (1992) Ocular effects of topical and systemic steroids. *Dermatol. Clin.* **10,** 505–512 Medline
86. Veenstra, D. L., Best, J. H., Hornberger, J., Sullivan, S. D., and Hricik, D. E. (1999) Incidence and long-term cost of steroid-related side effects after renal transplantation. *Am. J. Kidney Dis.* **33,** 829–839 CrossRef Medline
87. Costagliola, C., Cati-Giovannelli, B., Piccirillo, A., and Delfino, M. (1989) Cataracts associated with long-term topical steroids. *Br. J. Dermatol.* **120,** 472–473 CrossRef Medline
88. James, E. R. (2007) The etiology of steroid cataract. *J. Ocul. Pharmacol. Ther.* **23,** 403–420 CrossRef Medline
89. Urban, R. C., Jr., and Cotlier, E. (1986) Corticosteroid-induced cataracts. *Surv. Ophthalmol.* **31,** 102–110 CrossRef Medline
90. Dickerson, J. E., Jr., Dotzel, E., and Clark, A. F. (1997) Steroid-induced cataract: new perspective from *in vitro* and lens culture studies. *Exp. Eye Res.* **65,** 507–516 CrossRef Medline
91. Skalka, H. W., and Prchal, J. T. (1980) Effect of corticosteroids on cataract formation. *Arch. Ophthalmol.* **98,** 1773–1777 CrossRef Medline
92. Donshik, P. C., Cavanaugh, H. D., Boruchoff, S. A., and Dohlman, C. H. (1981) Posterior subcapsular cataracts induced by topical corticosteroids following keratoplasty for keratoconus. *Ann. Ophthalmol.* **13,** 29–32 Medline
93. Brocklebank, J. T., Harcourt, R. B., and Meadow, S. R. (1982) Corticosteroid-induced cataracts in idiopathic nephrotic syndrome. *Arch. Dis. Child.* **57,** 30–34 Medline
94. Oakley, R. H., and Cidlowski, J. A. (2013) The biology of the glucocorticoid receptor: new signaling mechanisms in health and disease. *J. Allergy Clin. Immunol.* **132,** 1033–1044 CrossRef Medline
95. Kwan, K. M., Fujimoto, E., Grabher, C., Mangum, B. D., Hardy, M. E., Campbell, D. S., Parant, J. M., Yost, H. J., Kanki, J. P., and Chien, C. B. (2007) The Tol2kit: a multisite gateway-based construction kit for Tol2 transposon transgenesis constructs. *Dev. Dyn.* **236,** 3088–3099 CrossRef Medline
96. Hayes, J. M., Hartsock, A., Clark, B. S., Napier, H. R., Link, B. A., and Gross, J. M. (2012) Integrin α5/fibronectin1 and focal adhesion kinase are required for lens fiber morphogenesis in zebrafish. *Mol. Biol. Cell* **23,** 4725–4738 CrossRef Medline
97. Yelon, D., Horne, S. A., and Stainier, D. Y. (1999) Restricted expression of cardiac myosin genes reveals regulated aspects of heart tube assembly in zebrafish. *Dev. Biol.* **214,** 23–37 CrossRef Medline
98. Hoage, T., Ding, Y., and Xu, X. (2012) Quantifying cardiac functions in embryonic and adult zebrafish. *Methods Mol. Biol.* **843,** 11–20 CrossRef Medline
99. Hill, E. G., Schwacke, J. H., Comte-Walters, S., Slate, E. H., Oberg, A. L., Eckel-Passow, J. E., Therneau, T. M., and Schey, K. L. (2008) A statistical model for iTRAQ data analysis. *J. Proteome Res.* **7,** 3091–3101 CrossRef Medline
100. Benjamini, Y., and Hochberg, Y. (1995) Controlling the false discovery rate–a practical and powerful approach to multiple testing. *J. R. Stat. Soc. B. Met.* **57,** 289–300